Journal of Power Sources 196 (2011) 6388–6393

Contents lists available at ScienceDirect

Journal of Power Sources

journal homepage: www.elsevier.com/locate/jpowsour

Co-doped NiO nanoflake arrays toward superior anode materials for lithium ion batteries

Y.J. Mai, J.P. Tu*, X.H. Xia, C.D. Gu, X.L. Wang

State Key Laboratory of Silicon Materials and Department of Materials Science and Engineering, Zhejiang University, Hangzhou 310027, China

ARTICLE INFO

Article history:
Received 7 January 2011
Received in revised form 28 March 2011
Accepted 29 March 2011
Available online 5 April 2011

Keywords:
Nickel oxide
Array film
Metal-doping
Electronic conductivity
Lithium ion battery

ABSTRACT

Co-doped NiO nanoflake arrays with a cellular-like morphology are fabricated by low temperature chemical bath deposition. As anode material for lithium ion batteries (LIBs), the array film shows a capacity of 600 mAh g^{-1} after 50 discharge/charge cycles at low current density of 100 mA g^{-1}, and it retains 471 mAh g^{-1} when the current density is increased to 2 A g^{-1}. Appropriate electrode configuration possesses some unique features, including high electrode–electrolyte contact area, direct contact between each naonflake and current collector, fast Li^+ diffusion. The Co^{2+} partially substitutes Ni^{3+}, resulting in an increase of holes concentration, and therefore improved p-type conductivity, which is useful to reduce charge transfer resistance during the charge/discharge process. The synergetic effect of these two parts can account for the improved electrochemical performance.

1. Introduction

Lithium ion batteries (LIBs) now dominate the portable electronic market, but they fall short of satisfying needs for high power and/or capacities for applications such as power tools, electronic vehicles or efficient use of renewable energies [1]. Conversion reactions of interstitial-free 3d metal oxides have been shown to be highly reversible, providing outstanding capacities to store lithium [2–12]. However, a major drawback of the conversion reactions is their poor kinetics related either to intrinsic poor electronic/ionic conductivity of the electrode materials or to inadequate means of configuring the electrodes.

Recently, self-supported nano-material arrays directly growing on current collector represent the feasibility of improving the kinetics. These electrodes show several unique advantages, such as high accessible surface area, easy accessibility, good cohesion to current collector, and features on the nanometer scale. Li et al. demonstrated that the mesoporous Co_3O_4 nanowire arrays on Ti foil as anodes for LIBs maintained a capacity of 700 mAh g^{-1} after 20 cycles at a current of 1 C, and retained 50% of the capacity when the current was increased to 50 C [13]. The self-supported Ni_3S_2/Ni nanoarchitectured electrode exhibited a sustained reversible capacity at 2 C with a loss of only 18% after 20 cycles [14]. Kim and co-workers reported that the self-supported SnS nanosheets possessed good cycling performance and superior rate capability of 380 mAh g^{-1} at 20 C [15].

Chemical bath deposition (CBD) is a prevalent low-temperature aqueous technique for directly depositing large-area thin film with self-supporting architecture of semiconductors [16–18]. In addition, it is theorized that if cation-deficient solid solutions could be retained, good p-type conductivity should result, which is well demonstrated by transition metal oxides [19–22]. In the special case of NiO, Co-doped NiO hexagonal nanoplatelets in the form of powder materials with improved electrochemical performance in the application of supercapacitor have been reported [23]. Moreover, the direct growth of self-support active materials on current collector is an important issue for their potential application in the next-generation LIBs.

Here, we report a one-step method for producing Co-doped NiO thin film by CBD with an appropriate adding amount of $CoSO_4$. The resulting electrode not only shows self-support nanoflake arrays but also possesses better electronic/ionic conductivities due to the doping of cobalt and nanoflake arrays. Using such electrodes, they show high capacity, good cycling performance and high rate capability. To the best of our knowledge, it is the first time to report Co-doped NiO self-support arrays fabricated by CBD toward electrode materials for LIBs.

2. Experimental

Co-doped NiO nanoflake arrays were synthesized by chemical bath deposition method modified from our previous reports [24,25]. Specifically, 38.8 mmol $NiSO_4$, 1.2 mmol $CoSO_4$ and

* Corresponding author. Tel.: +86 571 87952856; fax: +86 571 87952573.
E-mail address: tujp@zju.edu.cn (J.P. Tu).

0378-7753/$ – see front matter © 2011 Elsevier B.V. All rights reserved.
doi:10.1016/j.jpowsour.2011.03.089

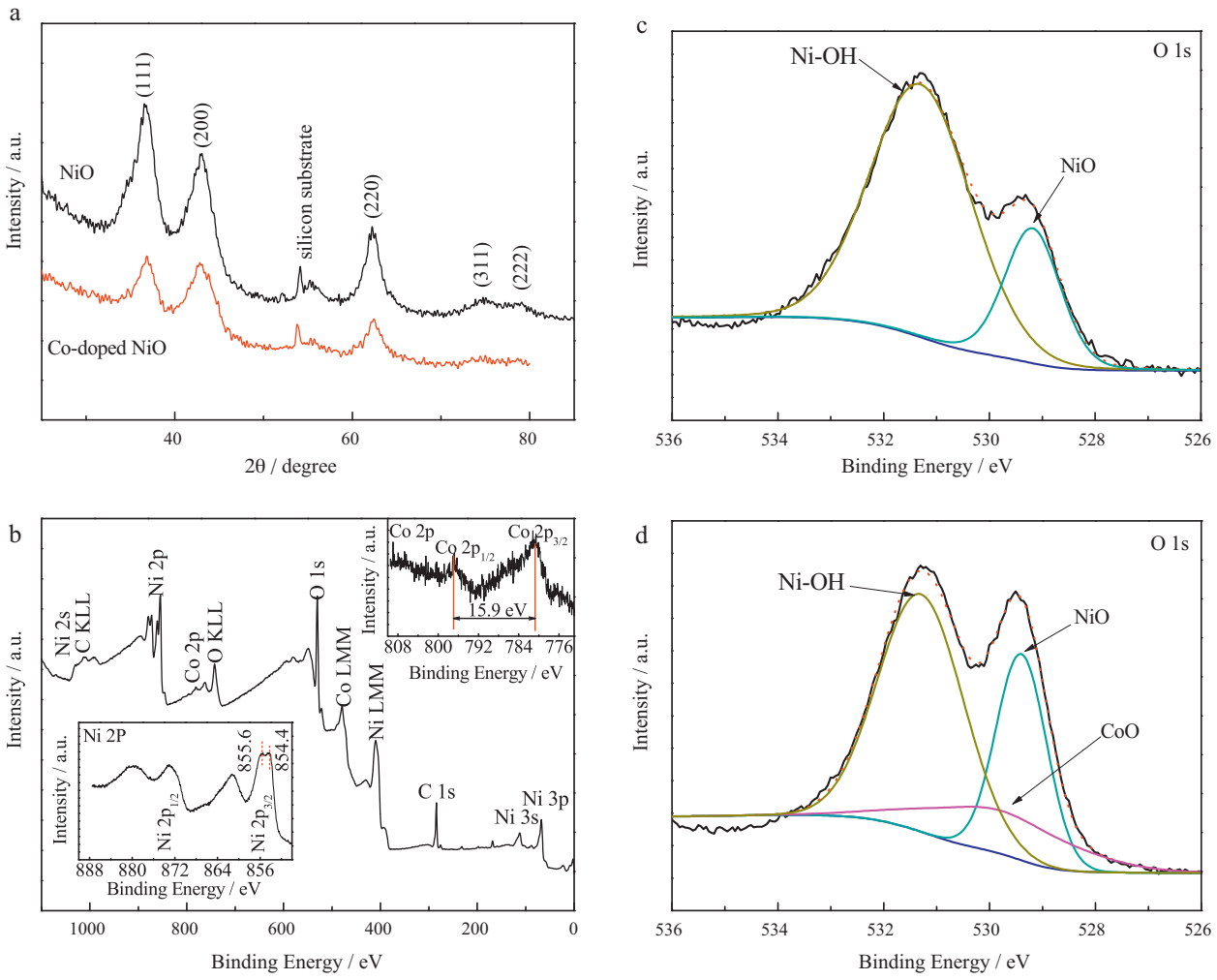

Fig. 1. XRD patterns of pure NiO and Co-doped NiO (a), and XPS wide spectrum of Co-doped NiO film (b), the insets are Ni 2p and Co 2p spectrum, respectively, O 1s spectrum of NiO (c) and Co-doped NiO (d).

7.4 mmol $K_2S_2O_8$ were dissolved in 10 ml of concentrated ammonia and 90 ml of deionized water. For comparison, pure NiO thin film was also prepared with the same process without addition of $CoSO_4$. After deposition on the pre-treated commercial Ti foil, the films were calcined in a tube furnace at 350 °C for 2 h in flowing argon. If the deposition time is 2 h, the thickness is about 980 nm for pure NiO film and about 360 nm for Co-doped NiO film, respectively. For comparison on their electrochemical performance, the deposition time is cut to 20 min for pure NiO film, resulting in nearly the same thickness of both films. Some samples were also deposited on silicon wafers and slides to facilitate characterization of XRD and measurement of Hall effect.

CR-2025-type coin cells were assembled in a glove box under argon atmosphere, where the as-prepared NiO electrodes were used as working electrodes and lithium foil as counter electrode and reference electrode. The electrolyte was 1 M $LiPF_6$ in ethylene carbonate (EC)–dimethyl carbonate (DME) (1:1 in volume). The galvanostatic charge–discharge tests were conducted on LAND battery program-control test system. Cyclic voltammetric (CV) measurements of the electrodes were performed on a CHI660C electrochemical workstation with a scan rate of 0.1 mV s^{-1} between 0 and 3 V (vs. Li/Li^+). The electrochemical impedance spectroscopy (EIS) of the electrodes was also carried out on CHI660C with a frequency range of 0.01 Hz to 100 kHz. Before the measurement, the electrodes were cycled for eight cycles, then discharged to 2.7 V and kept until the open-circuit voltage stabilized.

The microstructure, surface morphology and composition of the as-prepared NiO films were characterized by using X-ray diffraction (D/max 2550-PC), in which a glancing-angle mode with the incident beam at an angle of 4° was employed, X-ray photoelectron spectroscopy (XPS, AXIS UTLTRADLD equipped with a dual Mg Kα–Al Kα anode for photoexcitation) and field emission scanning electron microscope (FESEM, S-4800 coupled with EDX). Hall effect measurements were carried out on HL5500 Hall system.

3. Results and discussion

Fig. 1a shows the XRD patterns of NiO and Co-doped NiO films. The diffraction peaks of both films can be well assigned to face-centered-cubic (FCC) NiO (JCPDS 78-0643), and no obvious peaks for cobalt oxides or other impurities are detected, implying that the cobalt doping does not change the original NiO structure. Broader peaks in XRD pattern make it difficult to observe the obvious shift after the doping Co into NiO thin film. The corresponding XPS provides further structural information for the obtained films. Fig. 1b shows the XPS wide spectrum of Co-doped NiO film. Characteristic peaks in the inset of Fig. 1b represent Co 2p of CoO [26]. Ni $2p_{3/2}$ peak includes two components, one at 854.4 eV due to Ni–O bonds and the other one at 855.6 eV due to Ni–OH bands, respectively. The Ni–OH bands mainly come from nickel hydroxide α-$Ni(OH)_2$, β-$Ni(OH)_2$ and higher valence nickel oxides such as $Ni_2O_3{\cdot}H_2O$, β-NiO(OH), or $4Ni(OH)_2{\cdot}NiOOH{\cdot}xH_2O$ [16]. In O 1s spectrums, the

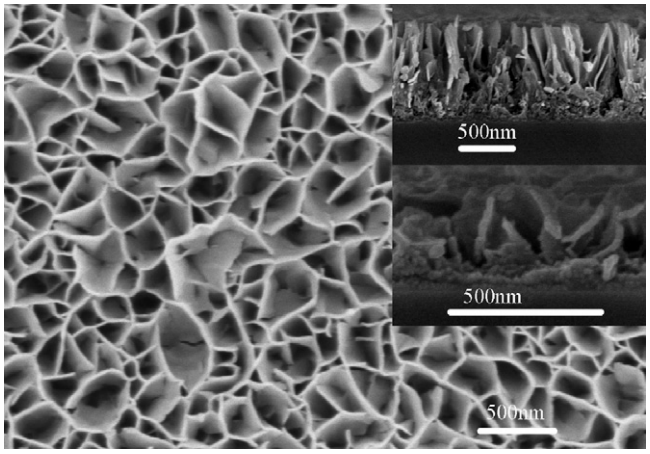

Fig. 2. SEM image of NiO films, the insets are cross-sectional images of pure NiO (up) and Co-doped NiO (down), respectively.

peak at 531.3 eV for pure NiO as well as Co-doped NiO indicates the presence of Ni-OH bands, which are consistent with Ni $2p_{3/2}$ spectrums. It is likely that the as-prepared films contain higher valence oxides because of the presence of persulfate. Comparing O 1s spectrum of pure NiO and Co-doped NiO film shown in Fig. 1c and 1d, respectively, we found, first, that the Co-doped NiO gives rise to one more O 1s peak at 529.6 eV, corresponding to CoO. Second, the intensity ratio of Ni–OH bands/NiO (NiO and CoO) bands obviously decreases after doping of cobalt. The Hall effect measurements suggested the obtained NiO film without cobalt doping was n-type which could be mainly attributed to the present of Ni^{3+} [21], although NiO was not n-dopable because of the spontaneous formation of electron killer [27]. The carrier concentration of pure NiO film was 1.93×10^{12} cm^{-3} with a mobility of 40.5 cm^2 V^{-1} s^{-1} as well as a resistivity of 8×10^4 Ω cm. After doping with Co, the as-prepared film transferred to p-typed due to Co^{2+} partially substitute Ni^{3+}. The concentration of majority carrier was 6.95×10^{15} cm^{-3}, coupled with a mobility of 17.2 cm^2 V^{-1} s^{-1} as well as a resistivity of 52.28 Ω cm. Based on the above results, it is reasonable to deduce that the as-prepared NiO films contain higher valence oxides consisting of $Ni_2O_3{\cdot}H_2O$, β-NiO(OH), or $4Ni(OH)_2{\cdot}NiOOH{\cdot}xH_2O$, and their amount is so small that beyond the detection limitation of XRD but XPS. After doping with Co, the Co^{2+} partially substituted Ni^{3+}, resulting in an increase of hole concentration, and therefore an enhanced p-type conductivity, which is useful to reduce the charge transfer resistance during the charge/discharge process. It is expected that the electrode materials with an enhanced intrinsic electronic conductivity should result in good electrochemical performance when they are applied to lithium ion batteries.

Fig. 2 shows the SEM image of Co-doped NiO nanoflake arrays film. The NiO film is uniform in appearance, exhibiting nanoflake arrays and cellular like morphology, which is the result of a competition between heterogeneous film growth on the substrate and homogeneous growth and aggregation leading to particle formation [16]. However, it is observed that no film appears under the same preparation condition of pure NiO thin film if $NiSO_4$ is replaced by $CoSO_4$. Neither raising temperature nor increasing the amount of oxidizer ($K_2S_2O_4$) can obtain film. Unless $CoSO_4$ decreases to a certain amount, the Co-doped NiO thin film will not be obtained, but particles. Second, the adding of $CoSO_4$ significantly affects the growth of NiO film, which can be confirmed by the film thickness obtained from the SEM images of cross section of both samples. This can be attributed that cobalt (II) hydroxide additive inhibits the transition from β-$Ni(OH)_2$ to γ-NiOOH [28], while ions with higher valence states are more prone to undergo hydrolysis and precipitate as hydroxides or oxides than those with

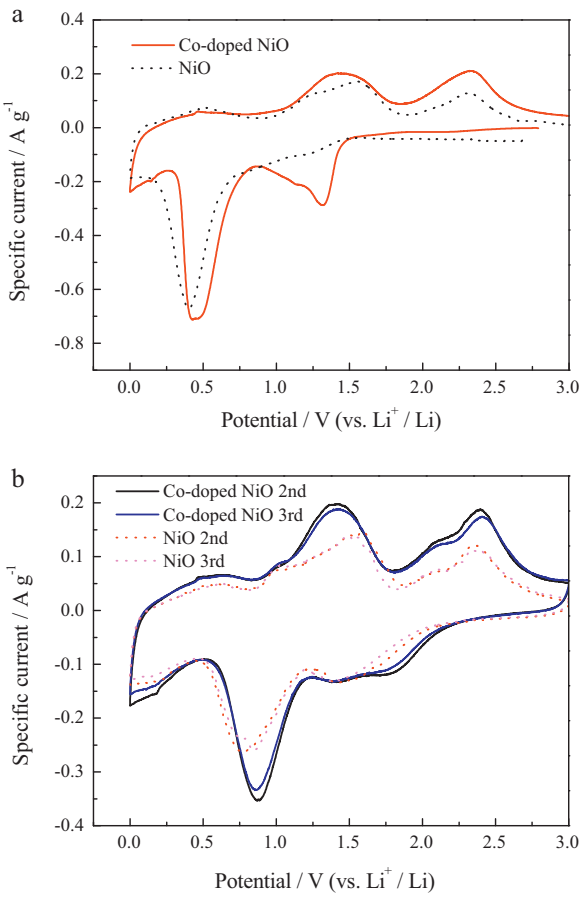

Fig. 3. CV curves of pure NiO and Co-doped NiO electrodes at a scan rate of 0.1 mV s^{-1} between 0 and 3.0 V: (a) the first cycle, (b) the second and third cycles.

lower valence states [29]. In addition, EDX analysis indicated the atomic ratio of Ni and Co is 9:1. It is noted that cobalt doping and post heat treatment do not change the morphology of the prepared films.

For comparison on the electrochemical performance, especially rate capability, we deliberately decreased the deposition time of pure NiO to 20 min to obtain an approximate thickness of both films (about 360 nm). The reaction mechanism of NiO by Li was well demonstrated in previous reports [2,30–33]. It first involved the formation of highly reactive nickel nanograins, which was the key to enable the formation-decomposition of Li_2O upon subsequent cycles, dispersed into Li_2O matrix, followed by the growth of an organic coating that partially dissolved upon the subsequent charge while Ni converted back to NiO nanograins. It can be described by the electrochemical conversion reactions [2]: $NiO + 2Li^+ + 2e \underset{\text{charge}}{\overset{\text{discharge}}{\rightleftarrows}} Li_2O + Ni$. The CV curves of pure NiO and Co-doped NiO electrodes, as shown in Fig. 3, reflect the above reaction mechanism. For the Co-doped NiO electrode in the first cycle (Fig. 3a), a main cathodic peak is observed at about 0.45 V and a low-intensity peak near 1.3 V correspond the reduction of NiO to metallic Ni nanoparticles and the formation of a partially reversible SEI layer whose composition includes Li_2CO_3, ethylene-oxide-based oligomers, LiF, and lithium alkyl carbonate [31,34]. Anodic peaks at around 0.5 V and 1.41 V correspond to the partial decomposition of the polymeric coating on the NiO surface, while the decomposition of Li_2O and nickel converted back to NiO nanograins for another anodic peak at 2.32 V. These results are consistent with previous reports [25,35]. For the pure NiO electrode,

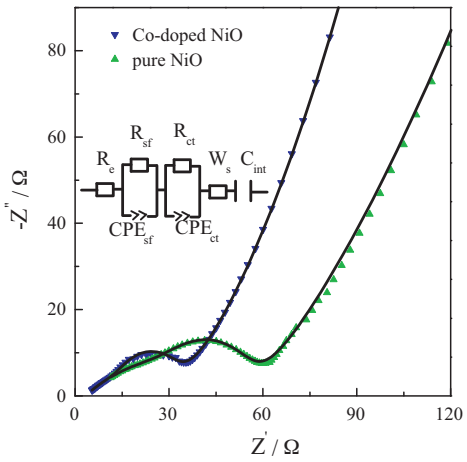

Fig. 4. Nyquist plots (the symbols) of both NiO electrodes and the fitted spectra (the continuous lines) in the potential of about 2.7 V (vs. Li/Li^+) after several discharge/charge cycles. The inset is the equivalent electrical circuit.

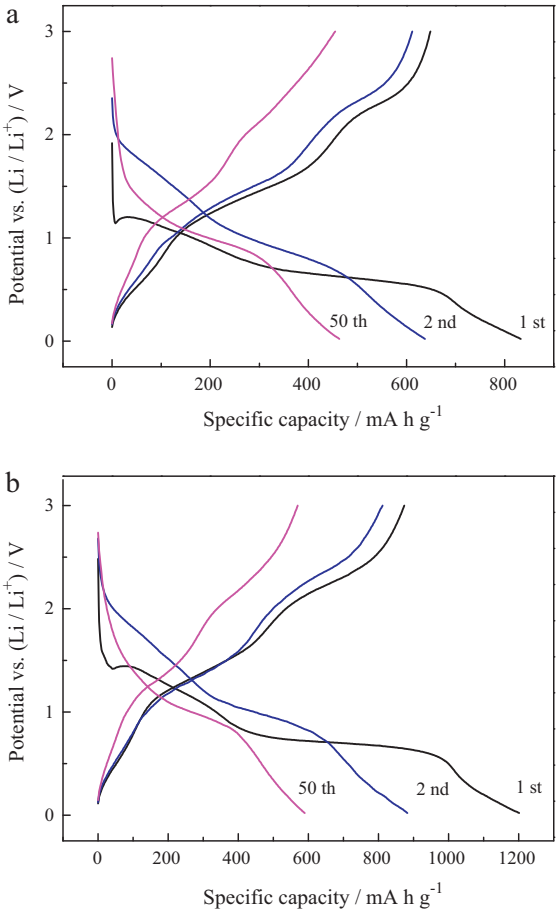

Fig. 5. Discharge–charge curves of (a) pure NiO; (b) Co-doped NiO.

the cathodic peak shifts to 0.39 V, and these anodic peaks shift to 1.56 and 2.33 V, respectively. It is found that in the first cycle, the intensity of cathodic peaks for Co-doped NiO electrodes at near 1.3 V is much stronger than that for pure NiO, which are mainly attributed to the improved electronic conductivity of Co-doped NiO electrode, facilitating the charge transfer needed for redox processes of solvent molecules in electrolyte relating to the formation of SEI layer. The integral area of anodic peak locating at near 1.41 V is larger than that for pure NiO electrode, indicating more dissolution of organic coating upon the subsequent charge for Co-doped NiO electrode. The separation between the reduction and oxidation peaks of the Co-doped NiO electrode decreases as compared to that of pure NiO electrode, indicating weaker polarization and better reversibility. This separation is also observed in the following cycles, as shown in Fig. 3b. In addition, the peak intensity and integral areas of the Co-doped NiO electrode are larger than those of pure NiO, indicating that more reactions toward Li^+ occur in the Co-doped NiO electrode. The incorporation of cobalt affects both the ionic and the electronic conductivity of the active material, result in a better electrode utilization and improvement of reaction kinetics [36], which is favorable in the application of supercapacitors [36,37].

The increased electronic conductivity after cobalt doping is further demonstrated by EIS. The Nyquist plots are shown in Fig. 4, whose data are analyzed by fitting to an equivalent electrical circuit (inset of Fig. 4). R_e, R_{sf} and R_{ct} represent the electrolyte resistance, surface film resistance and Li-ion charge transfer resistance at the interface between electrolyte and electrode, respectively. Given to the porosity of the measured materials, two constant phase element, CPE_{sf} and CPE_{ct}, were employed, instead of pure capacitances [38,39]. W_s and C_{int} correspond to diffusion components like Warburg impedance and the intercalation capacitance, respectively [40]. In Fig. 4, the symbols are the experimental data whereas the continuous lines represent the fitted spectra. For the pure NiO electrode, two semicircles are observed, including the depressed one located at near 9670 Hz, corresponding mainly to surface film resistance, and the other at about 300 Hz, corresponding mainly to Li-ion charge transfer resistance. The impedance spectra for Co-doped NiO electrode also show two depressed semicircle. However, the diameter of the second semicircle, reflecting the resistant of R_{ct}, reduces drastically, indicating that the latter possesses lower charge transfer resistance than pure NiO electrode. The curve fitting further confirms this assumption. It reveals the impedance of R_{ct} is $28.5 \pm 4.8\ \Omega$ for pure NiO electrode, whereas it reduces drastically to $19.6 \pm 0.3\ \Omega$ for Co-doped NiO electrode. R_{sf} is $38.3 \pm 3.4\ \Omega$ for pure NiO and $32.9 \pm 0.9\ \Omega$ for Co-doped NiO electrode.

The discharge/charge curves of pure NiO and Co-doped NiO electrode at low current density of 100 mA g^{-1} are shown in Fig. 5a and b, respectively. For the Co-doped NiO electrode, as shown in Fig. 5b, two plateaus and a sloping potential range during the first discharge/charge are well resolved. A narrow plateau at 1.5–0.9 V and a sloping part at 0.6–0.01 V during discharge correspond to the plateau at 1.0–1.5 V and the sloping part at 0.01–1.0 V during charge, indicating the formation and partially dissolution of a SEI layer, respectively; while a long discharge plateau at 0.6 V and a charge plateau at 2.0–2.5 V correspond to the reduction of NiO to metallic nickel nanoparticles dispersed into Li_2O matrix and its oxidation to NiO nanograins and decomposition of Li_2O. These results are agreed with the above CV results. Wang and co-workers reported that SEI layer had already started above 2.0 V during the first cathodic scan [41], and Tarascon and co-workers also observed the formation of SEI layer by ex situ TEM at the sloping potential range of 1 to 0.02 V [31]. What's more, it is well known that Ni and Co nanograins can act as the catalyst toward the formation/dissolution of the organic coating. So, it is reasonable to deduce that for the present electrode materials, the SEI layer starts at relative high potential of 1.3 V and further grows at lower potential (less than 0.5 V). And with the help of highly catalyst reactive of Co and Ni nanograins, the formed SEI layer partially dissolves upon the subsequent charge. The pure NiO electrode delivers 832.8 mAh g^{-1}, 637.5 mAh g^{-1} and 463.3 mAh g^{-1} for the 1st, 2nd and 50th cycle, respectively. The initial discharge specific capacity is 1201 mAh g^{-1} for the Co-doped NiO electrode. The discharge specific capacity decreases to 882.6 mAh g^{-1} in the

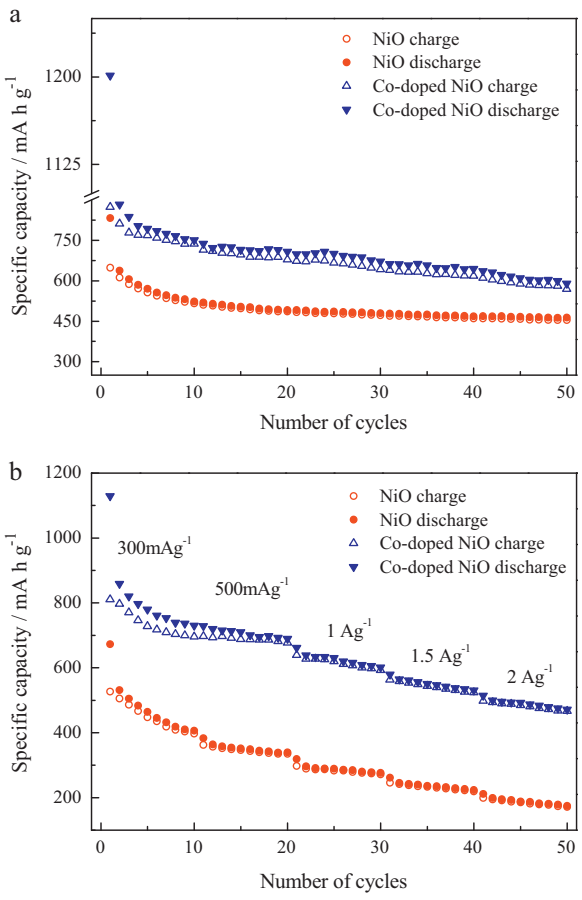

Fig. 6. Cycling performances of both NiO electrodes at a current density of 100 mA g^{-1} (a) and rate capability (b).

2nd cycle and remains at 589.5 mAh g^{-1} after 50 cycles. As shown in Fig. 6, the Co-doped NiO electrode has high specific capacities in spite of at a low current density (100 mA g^{-1}) or at a high current density (2 A g^{-1}) compared to the pure NiO electrodes. What's more, the Co-doped NiO electrode possesses excellent rate capability and shows good capacity retention even at higher current rates. Reversible and steady capacity of 471 mAh g^{-1} was achieved at a high current density of 2 A g^{-1}, whereas 174 mAh g^{-1} for the pure NiO electrode. To improve electrochemical performance of NiO in the application of LIBs, many attempts were operated, including ZnO–NiO–C film (230 mAh g^{-1}) [42], three-dimensional porous NiO (450 mAh g^{-1}) [41], core-shell structured Ni/NiO (about 200 mAh g^{-1}) [43], hierarchically ordered porous NiO (518 mAh g^{-1}) [44]. Compared with these previous attempts, the present method synchronously considers optimization design of electrode configuration and improvement of the lattice electronic conductivity of active materials and the Co-doped NiO electrodes show comparable capacities at low current density (100 mA g^{-1}), but better capacities and cycling performance at high current density (2 A g^{-1}).

It is suggested that the high capacity and rate capability of the Co-doped NiO electrode come from the unique hierarchical architecture combined with improved electronic conductivity after doping of Co^{2+}. The arrays configuration can facilitate the nanoflakes to participate in the electrochemical reaction because each nanoflake is directly in electric contact with the current collector. The open space between neighboring nanoflake allows for easy contact and diffusion of the electrolyte into the inner region of the electrode, and the thin thickness of flakes enables the high rate of lithium insertion/removal. In addition, the cobalt doping enhances p-type electronic conductivity of NiO, resulting in improved kinetics.

4. Conclusions

Co-doped NiO nanoflake arrays with a cellular-like morphology grown on Ti foil have been synthesized by CBD method. The addition of $CoSO_4$ significantly affects the growth of NiO film and an advisable adding amount of $CoSO_4$ is important to obtain the Co-doped NiO film. The Co-doped NiO electrode showed excellent rate capability and good capacity retention even at a high current rate of 2 A g^{-1}, with about 1.7 times improvement in the reversible specific discharge capacities compared to pure NiO. These improved electrochemical performances can be attributed to the synergetic effect coming from nanoflake array configuration, the open space and enhanced electronic conductivity after doping of cobalt. It also highlight our method is simple to synchronously obtain adequate electrode configuration and enhancement in the lattice electronic conductivity of NiO.

References

[1] P.L. Taberna, S. Mitra, P. Poizot, P. Simon, J.M. Tarascon, Nat. Mater. 5 (2006) 567–573.
[2] P. Poizot, S. Laruelle, S. Grugeon, L. Dupont, J.M. Tarascon, Nature 407 (2000) 496–499.
[3] M.K. Gulbinska, S.L. Suib, J. Power Sources 196 (2011) 2149–2154.
[4] P. Tartaj, J.M. Amarilla, J. Power Sources 196 (2011) 2164–2170.
[5] Y. Sun, X.-Y. Feng, C.-H. Chen, J. Power Sources 196 (2011) 784–787.
[6] P. Zhang, Z.P. Guo, Y.D. Huang, D.Z. Jia, H.K. Liu, J. Power Sources, doi:10.1016/j.jpowsour.2010.10.090.
[7] K.F. Zhong, B. Zhang, S.H. Luo, W. Wen, H. Li, X.J. Huang, L.Q. Chen, J. Power Sources, doi:10.1016/j.jpowsour.2010.10.031.
[8] X.H. Huang, J.P. Tu, B. Zhang, C.Q. Zhang, Y. Li, Y.F. Yuan, H.M. Wu, J. Power Sources 161 (2006) 541–544.
[9] M.-Y. Cheng, B.-J. Hwang, J. Power Sources 195 (2010) 4977–4983.
[10] J.Y. Xiang, J.P. Tu, L. Zhang, Y. Zhou, X.L. Wang, S.J. Shi, J. Power Sources 195 (2010) 313–319.
[11] X.H. Huang, J.P. Tu, C.Q. Zhang, X.T. Chen, Y.F. Yuan, H.M. Wu, Electrochim. Acta 52 (2007) 4177–4181.
[12] K.F. Zhong, X. Xia, B. Zhang, H. Li, Z.X. Wang, L.Q. Chen, J. Power Sources 195 (2010) 3300–3308.
[13] Y.G. Li, B. Tan, Y.Y. Wu, Nano Lett. 8 (2008) 265–270.
[14] Q. Wang, R. Gao, J.H. Li, Appl. Phys. Lett. 90 (2007) 143107.
[15] J.-G. Kang, J.-G. Park, D.-W. Kim, Electrochem. Commun. 12 (2010) 307–310.
[16] S.Y. Han, D.H. Lee, Y.J. Chang, S.O. Ryu, T.J. Lee, C.H. Chang, J. Electrochem. Soc. 153 (2006) C382–C386.
[17] J.C. Park, J. Kim, H. Kwon, H. Song, Adv. Mater. 21 (2009) 803–807.
[18] H.Y. Xu, S.L. Xu, H. Wang, H. Yan, J. Electrochem. Soc. 152 (2005) C803–C807.
[19] H.L. Pan, B. Yao, T. Yang, Y. Xu, B.Y. Zhang, W.W. Liu, D.Z. Shen, Appl. Phys. Lett. 97 (2010) 142101–142103.
[20] Y. Tsur, I. Riess, Ionics 1 (1995) 488–490.
[21] T. Dutta, P. Gupta, A. Gupta, J. Narayan, J. Appl. Phys. 108 (2010).
[22] D. Pasero, N. Reeves, A.R. West, J. Power Sources 141 (2005) 156–158.
[23] Z. Zheng, L. Huang, Y. Zhou, X.M. Hu, X.M. Ni, Solid State Sci. 11 (2009) 1439–1443.
[24] X.H. Xia, J.P. Tu, J. Zhang, X.L. Wang, W.K. Zhang, H. Huang, Electrochim. Acta 53 (2008) 5721–5724.
[25] X.H. Huang, J.P. Tu, X.H. Xia, X.L. Wang, J.Y. Xiang, L. Zhang, J. Power Sources 195 (2010) 1207–1210.
[26] S.C. Petitto, E.M. Marsh, G.A. Carson, M.A. Langell, J. Mol. Catal. A-Chem. 281 (2008) 49–58.
[27] S. Lany, J. Osorio-Guillen, A. Zunger, Phys. Rev. B 75 (2007) 241203.
[28] B.B. Ezhov, O.G. Malandin, J. Electrochem. Soc. 138 (1991) 885–889.
[29] H. Unuma, Y. Saito, K. Watanabe, M. Sugawara, Thin Solid Films 468 (2004) 4–7.
[30] L. Yuan, Z.P. Guo, K. Konstantinov, P. Munroe, H.K. Liu, Electrochem. Solid State Lett. 9 (2006) A524–A528.
[31] S. Grugeon, S. Laruelle, R. Herrera-Urbina, L. Dupont, P. Poizot, J.M. Tarascon, J. Electrochem. Soc. 148 (2001) A285–A292.
[32] P. Poizot, S. Laruelle, S. Grugeon, J.M. Tarascon, J. Electrochem. Soc. 149 (2002) A1212–A1217.
[33] B. Varghese, M.V. Reddy, Z. Yanwu, C.S. Lit, T.C. Hoong, G.V. Subba Rao, B.V.R. Chowdari, A.T.S. Wee, C.T. Lim, C.-H. Sow, Chem. Mater. 20 (2008) 3360–3367.
[34] G. Gachot, S. Grugeon, M. Armand, S. Pilard, P. Guenot, J.-M. Tarascon, S. Laruelle, J. Power Sources 178 (2008) 409–421.
[35] X.H. Huang, J.P. Tu, Z.Y. Zeng, J.Y. Xiang, X.B. Zhao, J. Electrochem. Soc. 155 (2008) A438–A441.
[36] A.B. Yuan, S.A. Cheng, J.Q. Zhang, C.N. Cao, J. Power Sources 77 (1999) 178–182.
[37] J.H. Park, S. Kim, O.O. Park, J.M. Ko, Appl. Phys. A-Mater. 82 (2006) 593–597.

[38] M.V. Reddy, S. Madhavi, G.V. Subba Rao, B.V.R. Chowdari, J. Power Sources 162 (2006) 1312–1321.
[39] M.D. Levi, D. Aurbach, J. Phys. Chem. B 108 (2004) 11693–11703.
[40] M.V. Reddy, T. Yu, C.H. Sow, Z.X. Shen, C.T. Lim, G.V. Subba Rao, B.V.R. Chowdari, Adv. Funct. Mater. 17 (2007) 2792–2799.
[41] C. Wang, D.L. Wang, Q.M. Wang, H.J. Chen, J. Power Sources 195 (2010) 7432–7437.
[42] Q.M. Pan, L.M. Qin, J. Liu, H.B. Wang, Electrochim. Acta 55 (2010) 5780–5785.
[43] X. Li, A. Dhanabalan, K. Bechtold, C. Wang, Electrochem. Commun. 12 (2010) 1222–1225.
[44] Y.F. Yuan, X.H. Xia, J.B. Wu, J.L. Yang, Y.B. Chen, S.Y. Guo, Electrochem. Commun. 12 (2010) 890–893.